

Atomistic Simulation of Water Percolation and Proton Hopping in Nafion Fuel Cell Membrane

Ram Devanathan,^{*,†} Arun Venkatnathan,[‡] Roger Rousseau,[†] Michel Dupuis,[†] Tomaso Frigato,[§] Wei Gu,^{||} and Volkhard Helms^{||}

Chemical & Materials Sciences Division, MS K2-01, Pacific Northwest National Laboratory, Richland, Washington 99352; Department of Chemistry, Indian Institute of Science Education and Research, Pune 411021, India; Institut für Mathematik, Freie Universität Berlin, Arnimallee 6, 14195 Berlin, Germany; and Center for Bioinformatics, University of Saarland, 66041 Saarbrücken, Germany

Received: April 15, 2010; Revised Manuscript Received: August 26, 2010

We have performed a detailed analysis of water clustering and percolation in hydrated Nafion configurations generated by classical molecular dynamics simulations. Our results show that at low hydration levels H_2O molecules are isolated and a continuous hydrogen-bonded network forms as the hydration level is increased. Our quantitative analysis has established a hydration level (λ) between 5 and 6 $\text{H}_2\text{O}/\text{SO}_3^-$ as the percolation threshold of Nafion. We have also examined the effect of such a network on proton transport by studying the structural diffusion of protons using the quantum hopping molecular dynamics method. The mean residence time of the proton on a water molecule decreases by 2 orders of magnitude when the λ value is increased from 5 to 15. The proton diffusion coefficient in Nafion at a λ value of 15 is about $1.1 \times 10^{-5} \text{ cm}^2/\text{s}$ in agreement with experiment. The results provide quantitative atomic-level evidence of water network percolation in Nafion and its effect on proton conductivity.

I. Introduction

Proton transport is a process of fundamental scientific interest and holds practical importance in a variety of research fields ranging from the study of biological proton pumps¹ to materials selection for polymer electrolyte membranes (PEMs) for fuel cells.² The latter has garnered growing attention, because of the promise of efficient conversion of chemical energy of fuel to electrical energy for portable power and transportation applications. A key component of PEM fuel cells is a polymer membrane of $\sim 100 \mu\text{m}$ thickness that conducts protons between the anode and cathode while separating the reactants (fuel and air). No existing membrane exhibits the desired combination of excellent proton conductivity, mechanical, and chemical stability, durability upon prolonged operation at high temperature and low humidity, and low cost needed for widespread adoption of this technology. There is thus a need to facilitate rational development of PEMs based on fundamental scientific understanding of membrane morphology, water distribution, and proton transport.

Several polymers have been studied as promising candidates for fuel cell membranes.² The most widely studied PEM for fuel cells is Nafion developed by DuPont Inc. It is suited for fuel cell operating temperatures below 85 °C, requires considerable hydration for good performance, and is considered a benchmark against which other membranes are evaluated. Chemically, Nafion is a random copolymer that consists of a hydrophobic poly(tetrafluoroethylene) (PTFE) backbone attached to a fully fluorinated pendant chain terminated with a strongly hydrophilic sulfonic acid group.³ The sulfonic acid

group is superacidic and evidence of its acidity is provided from infrared spectroscopy^{4,5} and from the first-principles calculations of Paddison.⁶ The main role of the sulfonic acid moiety is to enable conductivity of protons across the polymer membrane. Since the transport of protons is governed by the morphology and reactivity of membrane as well as the surrounding environment (e.g., water molecules), it is important to understand the transport of protons in the confined water environment of hydrated Nafion.

While it is widely understood³ that the hydrated Nafion membrane morphology consists of interconnected nanoscale hydrophilic domains in a hydrophobic background, the exact morphological details, such as domain shape and size, are topics of intense debate and scientific discussion. Many models based on spherical, rodlike, slab-type, and parallel cylindrical domains have been proposed,^{3,7} but the debate continues due to the inability of experiments, such as X-ray and neutron scattering, to unambiguously characterize the atomic-level details of membrane morphology. Even less is known about the morphology of novel membranes proposed in the literature. For the same reason, the dynamics of water molecules and protons are understood at the macroscale in terms of membrane conductivity as a function of hydration level,⁸ but detailed atomistic understanding that links the changes in distribution of water molecules to proton hopping in water with increase in membrane hydration is lacking. The hydration level is typically expressed as the number of H_2O molecules per SO_3^- group and is represented by λ .

Proton transport⁹ (PT) can be described as a combination of proton hopping (also known as Grotthuss¹⁰ or structural diffusion) among solvent molecules (e.g., water) and vehicular transport where protons diffuse in solution by forming a hydrated ion (e.g., hydronium ions). Both mechanisms are known to contribute to PT.¹¹ In order to study these mechanisms and understand how they contribute to the overall PT, it is necessary

* To whom correspondence should be addressed. E-mail: ram.devanathan@pnln.gov. Phone: 1-509-371-6487.

† Pacific Northwest National Laboratory.

‡ Indian Institute of Science Education and Research.

§ Freie Universität Berlin.

|| University of Saarland.

to use computational methods that can accurately describe these mechanisms. Molecular modeling and simulation has the potential to complement experimental studies and improve our atomic-level understanding of the dynamics of protons and water molecules in the complex chemical environment of the membrane. It should be noted that structural diffusion happens on faster time scales (up to a few picoseconds) whereas, vehicular diffusion occurs on slower time (nanoseconds) scales and different computational methods are required to study these mechanisms.

Modeling studies of PEM morphology and the transport of protons and small molecules have been reviewed recently,^{2,12} and a few representative examples of the modeling work are listed below. Quantum chemical calculations,^{6,12,13} ab initio metadynamics,¹⁴ first-principles molecular dynamics,^{15,16} empirical valence bond models,^{17–19} statistical mechanics,²⁰ classical molecular dynamics,^{21–30} and mesoscale models^{31,32} have been employed to understand proton transfer, proton transport, and water networks in hydrated Nafion. Paddison⁶ performed density functional theory (DFT) calculations on small membrane segments chosen to represent the pendant side chain of Nafion and found that proton transfer happens when there are three or more H₂O molecules per acidic pendant. Paddison and Elliot¹³ also performed a DFT study of the “short side chain” perfluorosulfonic acid membrane and found that the number of water molecules required for proton transfer also depends on the number of separating PTFE units of the backbone. A recent ab initio metadynamics¹⁴ study of hydrated pendants has also provided insights into the initial steps during the proton transfer.

Ab initio molecular dynamics (AIMD)^{15,16} studies have been performed for durations of 6–20 ps at two different values of λ . Simulations over a much longer time scale (\sim 1 ns) are needed for reliable results on PT. Due to steep computational cost, AIMD studies of large hydrated polymer systems with sampling over long time (nanoseconds) scales are currently out of reach, although steady improvements in computational power give cause for optimism. The integration of ab initio and classical MD methods is needed to study the transfer and transport of protons. Spohr et al.^{17,18} have used a two-state empirical valence bond (EVB) method to study proton mobility in a model PEM. Petersen et al.¹⁹ studied proton solvation in hydrated Nafion by a self-consistent iterative multistate EVB model. The authors have compared contributions from structural and vehicular diffusion of proton for two values of λ and at a single temperature (300 K). This study showed that the sulfonate ion acts as a proton trap. According to a statistical mechanical study,²⁰ the mobility of a proton is higher when it is much farther from a sulfonate group.

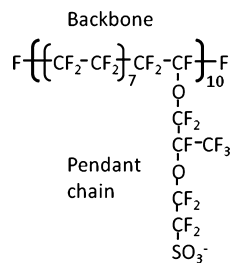
Certainly, sampling at nanosecond time scales is required to study the vehicular diffusion of protons in its hydrated form (e.g., hydronium ions). Classical MD simulations have therefore been extensively used to investigate the structural properties of Nafion membrane as well as vehicular diffusion of the hydrated proton and water molecules. Vishnyakov and Neimark²¹ used classical MD simulations to analyze the local structure of the solvent around the sulfonate group. Their results suggest that there is no percolating water network, but instead isolated water clusters are transiently connected by temporary water bridges. The dynamics of water molecules has been investigated by Urata et al.²² They observed that sulfonic groups are the only sites of the polymer to which water molecules are attracted. The use of classical MD simulations was further explored by Jang et al.²³ to compute the structural properties of Nafion membrane and dynamical properties of hydronium ions and water molecules

though their work was confined to two temperatures and a single value of λ . Blake et al.²⁴ observed percolation of the hydrophilic phase as λ increased in contrast to the findings of Vishnyakov and Neimark.²¹

Previously, we have used classical MD simulations^{25–27} to characterize the nanostructure of Nafion membranes and their dynamical properties such as diffusion coefficients and residence times of hydronium ions and water molecules from a dry state to an extremely wet state of the membrane and at different temperatures. Our previous work^{25–27} on the Nafion membrane has also shown that the vehicular transport of protons is strongly dependent on λ and fuel cell operating temperature. These classical MD simulations have allowed us to characterize the polymer membrane nanostructure and the dynamics of water in these systems, all with reasonable agreement with experiments. Recently, Knox and Voth²⁸ have used large-scale MD simulations to compare different morphological models of Nafion at two different values of λ , and observed the occurrence of water network percolation in all models. Cui et al.^{29,30} have used united atom force fields to study the aqueous phase structure in hydrated Nafion and short side-chain (SSC) perfluorosulfonic acid membranes. In Nafion, these authors observed a single large cluster of water molecules for λ values of 8.6 and 11.8. They also found that the water cluster distribution is less dispersed in Nafion compared to that in SSC membrane. Wescott et al.³¹ used a coarse-grained mesoscale modeling with interaction parameters generated by MD simulations to model water percolation in hydrated Nafion. However, the model could not resolve the atomistic details relevant to the percolation process. Malek et al.³² performed coarse-grained simulations of hydrated Nafion for four values of λ , namely 2, 4, 9, and 15, and determined water percolation to occur at a threshold λ of 4.

In the present work, we have performed a detailed analysis of water clustering and percolation in configurations of hydrated Nafion generated by all-atom classical molecular dynamics for λ values of 1, 3, 5, 7, 9, 11, 13.5, and 20 to determine the percolation threshold. Experimental studies³³ show that the maximum water sorption capacity of Nafion corresponds to a λ value of about 16. Thus, the λ values examined here represent the complete range from dry to fully saturated Nafion. We have chosen Nafion 117 (henceforth referred to as Nafion; 117 refers to an equivalent weight of 1100 g with a membrane thickness of 175 μm) for the present study of structural transport. The percolation analysis, based on the method of Brovchenko et al.,³⁴ is connected to proton mean residence times in hydrated Nafion obtained using the quantum hopping (Q-HOP) MD method.³⁵ QHOP-MD has been successfully used to study dynamic proton equilibria in condensed phases,^{35–37} proton exclusion in aquaporin-1 water channels,³⁸ the proton shuttle in green-fluorescent protein,³⁹ and the role of water wires in proton uptake by biological proton pumps.¹ A similar method has been previously used by Jang and Goddard⁴⁰ to study proton hopping in PEMs.

Q-HOP MD³⁵ allows stochastic proton hopping among flexible multiple protonation sites in the framework of conventional MD, with proton hopping probabilities parametrized on the basis of quantum mechanically derived proton transfer rates. The diffusion coefficient of an excess proton in water at 300 K was reported³⁵ as $(9.3 \pm 1.4) \times 10^{-5} \text{ cm}^2/\text{s}$ in excellent agreement with the experimental value of $9.3 \times 10^{-5} \text{ cm}^2/\text{s}$. More recently, Q-HOP MD method has been applied to study the dynamic protonation equilibrium of acetic acid³⁶ over a time scale of 50 ns. The authors concluded that an advantage of using the Q-HOP MD methodology is that PT pathways are automati-

**Figure 1.** Chemical structure of a single chain of Nafion.

cally provided using Q-HOP MD simulations without imposing any constraint on the PT pathway. Due to its general parametrization scheme, Q-HOP MD is, in principle, applicable to a wide range of systems including protein and polymer systems. We extend here the application of the Q-HOP MD method to study PT in hydrated Nafion. The implementation and parametrization of the Q-HOP method used here has been presented in detail previously.^{35,36,41,42} Hence, only the computational details of the Q-HOP MD simulation are presented below, followed by a discussion of results, and finally a summary of our findings.

II. Computational Details

A. Water Network Percolation Analysis. We performed classical MD simulations of hydrated Nafion using the DL_POLY code,⁴³ DREIDING⁴⁴ force field for Nafion, and F3C⁴⁵ force field for H₂O molecules and H₃O⁺ ions. We have presented the details of our simulation previously.^{26,27} The chemical structure of a single chain of Nafion (10 SO₃⁻ groups) is shown in Figure 1. Our simulation cell contained four chains of Nafion (40 SO₃⁻) with hydrophilic pendants spaced evenly by seven nonpolar ($-CF_2-CF_2-$) monomers that form a hydrophobic backbone. We have also performed simulations using 8 and 48 chains and found the structure and dynamical properties to be similar to that of the 4-chain system. In the present report, we will discuss water percolation in the 4-chain system, because it corresponds to the largest number of λ values studied, namely $\lambda = 1, 3, 5, 7, 9, 11, 13.5$, and 20. We generated the four Nafion chains of 682 atoms each by linking the polar monomeric unit to the end of the nonpolar monomeric unit, repeating the procedure nine times and terminating the two ends of the chain with F. To ensure charge neutrality, we added 40 H₃O⁺ ions and solvated the membrane by adding water molecules corresponding to a given λ . We did not impose any particular geometrical distribution of water molecules. The number of water molecules ranges from 0 for $\lambda = 1$ to 760 for $\lambda = 20$.

We used energy minimization and annealing to equilibrate the system as discussed previously.²⁶ After equilibration, the density of hydrated Nafion was comparable to experimental values.³³ Subsequently, we performed MD simulations for 2 ns in the constant NVT ensemble at 300 K with 1 fs time steps and saved the configurations every 0.2 ps. The range of λ values was chosen to critically examine the evolution of membrane morphology with increasing hydration. Experimental studies⁴⁶ have shown an abrupt change in the dielectric constant of Nafion between $\lambda = 6$ and $\lambda = 9$ coinciding with a significant increase in the proton diffusion coefficient.⁸ In order to obtain quantitative information about the change in water network with increasing λ , we have performed detailed percolation analysis.

Our analysis considers H₂O molecules and H₃O⁺ ions to be part of the same cluster if the oxygen atoms are separated by less than 3.5 Å. We calculated the cluster size distribution n_S , defined as the occurrence probability of clusters of size S

TABLE 1: Range of Maximum Cluster Sizes from 2000 Nafion Configurations at Each Hydration Level

hydration level (λ)	range of max water cluster size	total no. of H ₂ O molecules and H ₃ O ⁺ ions (N)
1.0	1	40
3.0	11 to 34	120
5.0	47 to 199	200
7.0	114 to 280	280
9.0	289 to 360	360
11.0	420 to 440	440
13.5	531 to 540	540
20.0	787 to 800	800

(measured by the number of H₂O molecules and H₃O⁺ ions in the cluster), as an average over 2000 configurations at an interval of 1 ps. n_S should decrease monotonically with increasing S well below the percolation threshold, show a peak at high S near the threshold, and show a sharp increase near the highest possible S value well above the threshold in finite size systems. However, this may not be a sensitive measure of the percolation threshold.^{34,47}

The mean cluster size of all but the largest cluster in the system, S_{mean} , was calculated as

$$S_{\text{mean}} = \frac{\sum n_S S^2}{\sum n_S} \quad (1)$$

where the sum is over all clusters excluding the largest. In a finite-sized system, S_{mean} is known to pass through a maximum just below the percolation threshold.³⁴ In fact, S_{mean} can be fitted⁴⁸ to

$$S_{\text{mean}} = A|\lambda - \lambda_p|^{-\nu} \quad (2)$$

to determine the percolation threshold λ_p . Here A is a constant and ν is a characteristic exponent. Unlike previous simulation studies of hydrated Nafion, the present simulations have examined a large number of λ values, which enables determination of λ_p by fitting to eq 2.

Other measures of percolation include the spanning probability P_s and the percolation probability P_p . We define P_s as the probability that the maximum cluster size in a given configuration is greater than $N/2$, where N is the total number of H₂O molecules and H₃O⁺ ions in the simulation cell. The value of N is given in Table 1 for the values of λ studied. P_p is defined as the probability that a H₂O molecule or H₃O⁺ ion will be in a cluster of size greater than $N/2$. The λ value at which P_s exceeds 0.95 can be taken as the upper bound of λ_p .⁴⁷

B. Quantum Hopping Molecular Dynamics. Q-HOP MD simulations of hydrated Nafion were performed using a modified version of NWChem 4.7.^{49,50} A single unit of Nafion, as shown in Figure 1, is made of a $-O-CF_2-C(F)(CF_3)-O-CF_2CF_2-$ SO₃⁻ pendant, and a perfluorinated backbone to which this pendant is attached. The construction of Nafion membrane has been described in detail in our earlier work.²⁵ In order to perform Q-HOP MD simulations on hydrated Nafion, three model systems were generated using the final configuration from the annealing procedure as described in our previous work.²⁵ This configuration consisted initially of a single Nafion chain with 10 SO₃⁻ groups, 10 H₃O⁺ ions, and 156 SPC/E⁵¹ H₂O molecules. We removed all the H₃O⁺ ions from this configuration to generate a template for creating configurations that

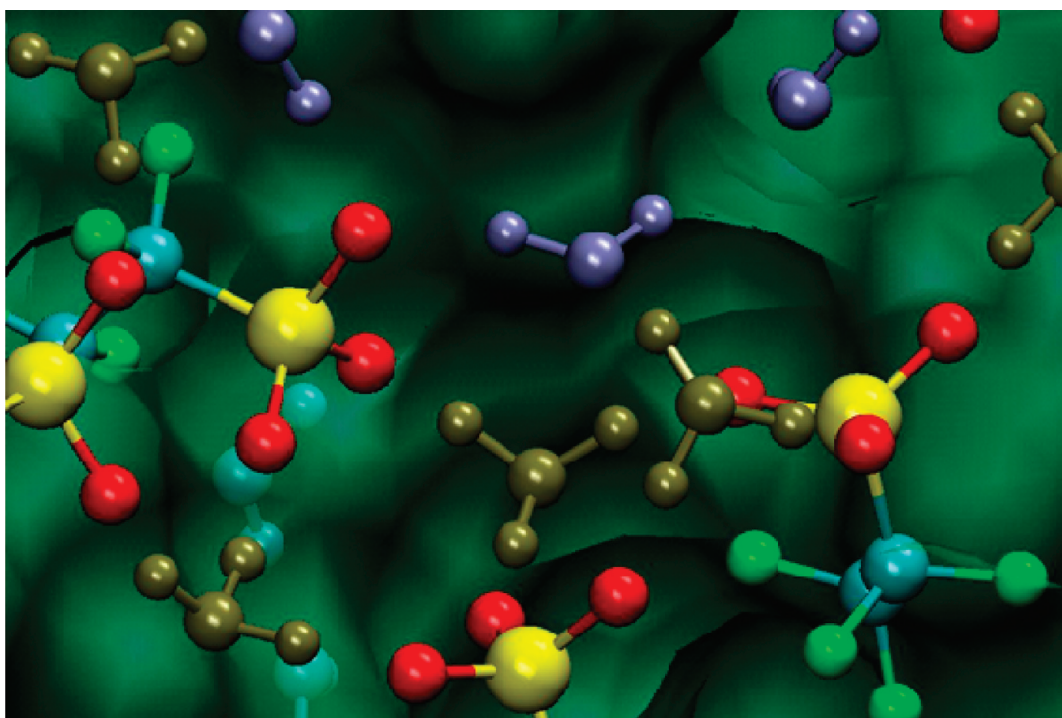


Figure 2. H_2O molecules (purple), H_3O^+ ions (tan), pendant chains (S in yellow, O in red, C in blue and F in green), and backbone (shown as a surface) at $\lambda = 3$. The H_2O molecules and H_3O^+ ions are bound by the SO_3^- groups at low hydration.

vary in water content. Using the template, three configurations were created such that each configuration consisted of a single Nafion chain but differed in the number of H_2O molecules (50, 100, and 150 H_2O molecules, respectively). Each configuration was replicated in space four times so that the replicated configurations contained 200, 400, and 600 H_2O molecules, respectively. The replicated model systems correspond to λ values of 5, 10, and 15, respectively. To ensure charge neutrality in the 4-chain Nafion system with 40 SO_3^- groups, 40 SPC/E⁵¹ H_2O molecules in each model were mutated to form 40 H_3O^+ ions.

The Q-HOP simulations of this work used exactly the same implementation and parametrization as the Q-HOP method described in the literature.^{36,37} For details of the parametrization, the reader is referred to the extensive online supplementary materials of ref 36. Protons residing on 39 H_3O^+ ions remained fixed and were not allowed to hop during the entire Q-HOP MD simulation. However, the proton residing on the remaining H_3O^+ ion was allowed to hop among the remaining H_2O molecules. The restriction of hopping of a single proton among H_2O molecules is the simplest extension of the vehicular diffusion-only model. A similar restriction was also used in the work of Petersen et al.¹⁹ This limitation can have an effect on proton dynamics, especially at low hydration levels. By having only one hopping proton, the influence of a proton hop on the hopping of another proton, stepwise proton transfer, and concerted proton transfer are ignored. Such processes can play a significant role in proton transport under low hydration levels and in confined environments.^{17,18} Under the current Q-HOP implementation in NWChem,^{49,50} the system temperature may become unstable when simulating a system containing extremely high concentrations of hoppable protons. In future work, we will develop a more robust implementation of the Q-HOP method to address this issue. Nevertheless, the simulations with one hoppable proton shown here are not affected by such issues so that the present simulations provide quantitative information

about proton transport in Nafion and relate it to water percolation within the limits of available computational capabilities.

The configurations generated using the above procedures were used as an input for Q-HOP MD simulations at 300 and 350 K. Each configuration was equilibrated for 200 ps, and the final structure obtained from the equilibration was used as an input for a 2 ns Q-HOP MD simulation using the NPT ensemble. Simulations of this length are not currently feasible with ab initio molecular dynamics for this system. The interatomic forces required for the Q-HOP MD simulation were computed using the AMBER 99/GAFF force field.^{52,53} The leapfrog Verlet algorithm⁵⁴ was used as the integrator to solve the equations of motion. The partial charges on the hydronium ions were -0.749 for oxygen atom and 0.583 for each hydrogen atom. The partial charges and force field parameters for the Nafion membrane have been discussed previously.²⁵ The trajectories and proton transfer information recorded during the course of the Q-HOP MD simulation were used to compute dynamical properties like residence times, rate constants, activation energies, mean square displacement, and diffusion of protons and H_3O^+ ions.

III. Results and Discussion

The morphology of hydrated Nafion membrane and the dynamics of H_2O molecules and H_3O^+ ions produced by AMBER^{52,53} and SPC/E⁵¹ force fields using the NWChem^{49,50} code are comparable to the corresponding results obtained with DREIDING⁴⁴ and F3C⁴⁵ force fields using the DL_POLY⁴³ code. For instance, Figure 2 shows a “bridging” structure that is obtained for $\lambda = 3$ using DREIDING⁴⁴ and F3C.⁴⁵ H_3O^+ ions are coordinated by multiple SO_3^- groups and form bridges between them. There is steric hindrance to the diffusion of H_3O^+ ions. Thus, H_2O molecules and H_3O^+ ions are bound to the end of the Nafion pendant, which is not conducive to proton transport. Such characteristic structures were also observed for $\lambda = 3.5$ using the AMBER^{52,53} and SPC/E⁵¹ force fields. It is important to point out that we did not impose the formation of

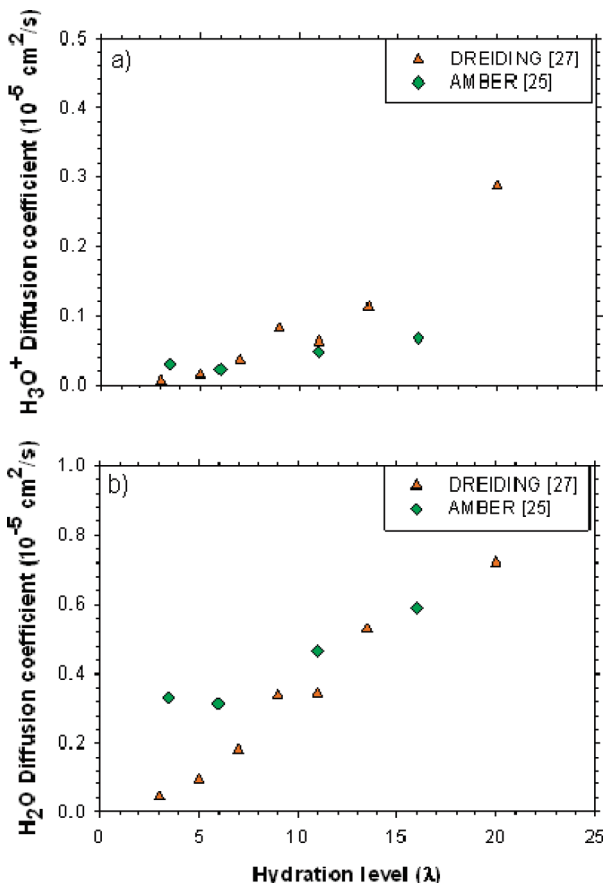


Figure 3. Comparison of diffusion coefficients of (a) H_3O^+ ions and (b) H_2O molecules obtained using two different sets of potentials.

complexes containing SO_3^- and H_3O^+ , for instance by starting the simulation with such a configuration. The water molecules and hydronium ions were allowed to migrate freely. In fact, even at a low hydration level of $\lambda = 3$, H_2O molecules migrate outside the first coordination shell of the SO_3^- group from time to time. Figure 3 compares the diffusion coefficients of H_3O^+ ions and H_2O molecules using the DREIDING⁴⁴ and AMBER^{52,53} force fields for Nafion. There is general agreement in the data except at the lowest λ for H_2O molecules and highest λ for H_3O^+ ions. The general features of Nafion morphology and molecular transport in Nafion membrane appear to be independent of the models and codes used.

The changes in the structure of the aqueous phase in Nafion with increasing hydration level can be understood by examining the water network connectivity. Figure 4 shows the cluster size distribution n_S for λ values of 3, 5, 7, and 9. For the purpose of this analysis, isolated molecules/ions are also considered clusters of size $S = 1$. n_S is expected to obey a power law of the form

$$n_S = CS^{-\tau} \quad (3)$$

where C is a constant and τ is 2.2 for three-dimensional percolation. The power law corresponding to this exponent is shown as a line in Figure 4. Since the curve tends to show a peak at high values of S as we approach the percolation threshold, only a limited range of values can be fitted to eq 3. The broader the range, the closer one is to the threshold. For $\lambda = 3$, we were able to fit the range from $S = 3$ to $S = 31$ with $\tau = 2.9$. For $\lambda = 5$, we were able to fit the widest range in this system from $S = 2$ to $S = 199$ with $\tau = 1.6$. The broad range

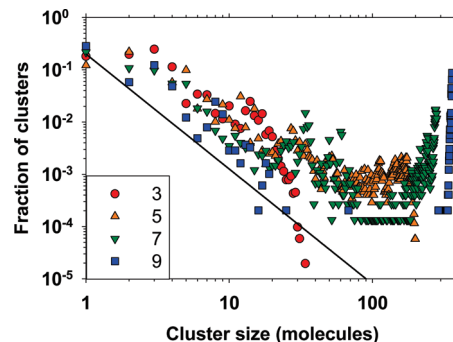


Figure 4. Cluster size distribution n_S for four hydration levels (λ) in Nafion. The line represents a power-law slope of -2.2 for three-dimensional percolation. The percolation threshold is close to $\lambda = 5$.

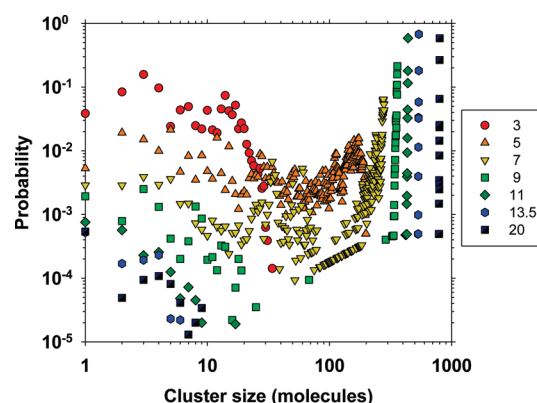


Figure 5. Probability of finding a H_2O molecule or H_3O^+ ion in a cluster of a given size for various hydration levels (λ) in Nafion. Percolation occurs between $\lambda = 3$ and $\lambda = 7$.

of S values fitted shows that, of the values of λ considered here, 5 is the closest to λ_p .

The percolation threshold can also be studied by calculating the probability, P_c , of finding H_2O molecules and H_3O^+ ions in a cluster of a certain size. Figure 5 is a plot of P_c as a function of λ values from 3 to 20. We do not show the data for $\lambda = 1$, because all the data points are at (1.0, 1.0). In other words, we observed 40 different H_3O^+ ions bound to individual SO_3^- groups for every configuration. The representation of the system using H_3O^+ ions at $\lambda = 1$ is an approximation, because the proton is known to reside on the sulfonate group at such a low hydration level.^{13,14} As in the case of n_S , we see that P_c decreases monotonically for $S > 10$ in the case of $\lambda = 3$, shows a peak at a high value of S of 174 for $\lambda = 5$, and shows a spike at the highest possible S value for λ from 7 to 20. From the trends in P_c , we can conclude that λ_p lies between $\lambda = 3$ and $\lambda = 7$. This can be verified from the average number of clusters plotted as a function of λ in Figure 6. We observe an order of magnitude decrease in the average number of clusters from 25.51 at $\lambda = 3$ to 3.73 at $\lambda = 7$. It is worth noting that an isolated ion would be considered a cluster in counting clusters, which is why the number of clusters is 40 (equal to the number of H_3O^+ ions) at $\lambda = 1$. Lu et al.⁴⁶ have reported an abrupt increase in the dielectric constant of hydrated Nafion around $\lambda = 6$. The present simulations show that there is a drastic decrease in the number of water clusters between $\lambda = 3$ and $\lambda = 7$, which provides an explanation for the experimentally observed property changes⁴⁶ in terms of water network percolation.

The formation of a spanning water network for $\lambda > 5$ can be visualized in Figure 7, which presents perspective projections of the membrane at various hydration levels. H_2O molecules

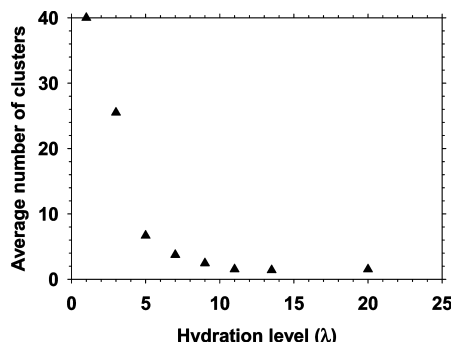


Figure 6. Average number of clusters in hydrated Nafion. Each isolated ion/molecule is also counted as a separate cluster in this analysis.

and H_3O^+ ions are shown (O in red, H in white) in ball and stick representation, the SO_3^- group is shown as a large yellow bead, and the rest of the pendant and the backbone are shown as a transparent surface. At a low hydration level corresponding to $\lambda = 3$, we observe isolated clusters. The spatial extent of the clusters increases at $\lambda = 5$, but the clusters do not percolate. For $\lambda = 7$, a large spanning cluster is seen. At the highest hydration level shown ($\lambda = 13.5$), three-dimensional percolation is evident. The representation of the membrane as a transparent surface facilitates the visualization of water network connectivity in the direction perpendicular to the viewing surface. As discussed by Knox and Voth,²⁸ the SO_3^- groups appear to play an important role in percolation by penetrating the H_2O clusters and facilitating the aggregation of H_2O molecules. The SO_3^- end of the pendant is hydrophilic and extends away from the rest of the membrane, which is hydrophobic, into the water channels as seen in Figure 2. H_2O molecules form dynamic linkages between these hydrophilic domains. Our previous simulations²⁷ have showed that the H_2O molecules are highly mobile. Thus, the percolating network is not a static entity, but is made of diffusing H_2O molecules that enable vehicular and structural transport of protons.

The development of this percolation network can be further analyzed in terms of the number of water molecules present in the smallest and largest clusters. Figure 8 is a plot of the probability of finding a H_2O molecule or H_3O^+ ion in the five smallest possible clusters (S ranging from 1 to 5) and the five largest possible clusters (S ranging from $N - 4$ to N) as a function of hydration level. Lines have been drawn through the data points to guide the eye. At $\lambda = 1$ or 3, H_2O is much more likely to occur in the five smallest sizes than in the five largest sizes. For $\lambda = 5$, H_2O is more likely to occur in the five smallest than in the five largest clusters, but the combined probability of occurrence in these 10 clusters is less than 0.1. Most of the H_2O molecules are in intermediate sized clusters. As λ increases above 7, the largest size clusters become increasingly more probable than the smallest. At $\lambda = 11$, the combined probability of finding a H_2O molecule in $1 \leq S \leq 5$ is less than 0.002, while that of $N - 4 \leq S \leq N$ is greater than 0.96. The crossover between the two curves is at $\lambda = 5.5$. On the basis of this observation, we propose a new criterion for the detection of the percolation transition, namely the crossover of the curves corresponding to the probability of finding H_2O in the five smallest possible and five largest possible clusters. The choice of five clusters is arbitrary. If the 10 largest and smallest clusters are considered, the crossover is at $\lambda = 5.3$. If the probability of occurrence in the two smallest ($S = 1$ or 2) and two largest ($S = N - 1$ or N) possible clusters are considered, the curves crossover at $\lambda = 5.9$. On the basis of this criterion, we can conclude that percolation occurs between $\lambda = 5$ and $\lambda = 6$.

In addition to the criteria discussed above, it is useful to study the variation of the percolation probability (P_p) and spanning network probability (P_s) as a function of hydration level as shown in Figure 9. Lines are drawn through the data points to guide the eye. Both P_p and P_s are zero for $\lambda = 1$ and $\lambda = 3$. P_s reaches 0.99 at $\lambda = 7$ and is 1.0 at higher λ . P_p lies between 0.99 and 1.0 for $\lambda \geq 9$. By curve fitting, one can determine that $P_s = 0.95$ is attained for $\lambda \sim 5.7$. This value of λ_p is consistent with the preceding estimates. Another reliable measure of λ_p can be obtained by fitting the variation of S_{mean} with λ to eq 2. Figure 10 shows a plot of S_{mean} as a function of λ from the present simulation. For $\lambda < \lambda_p$, S_{mean} increases with hydration level, because larger clusters start to appear. Even after exclusion of the largest cluster, the average cluster size increases. For $\lambda > \lambda_p$, S_{mean} decreases with hydration level, because intermediate-size clusters are increasingly absorbed into the largest cluster and this large cluster is excluded from the calculation of S_{mean} . By fitting the entire range of λ values to eq 2, we obtain $\lambda_p = 5.93$ and $\nu = 1.42$. Since we have more data points above λ_p than below, we also tried fitting only the points corresponding to $\lambda \geq 7$. This fit resulted in $\lambda_p = 5.90$ and $\nu = 1.81$.

Table 1 lists the range of maximum cluster sizes observed in 2000 configurations for each value of λ and sheds light on the persistence of the percolation network. At $\lambda = 1$, the H_3O^+ ions are bound and only one cluster size ($S = 1$) is possible. At $\lambda = 3$, the largest cluster size encountered during the simulations is 34. This is not a spanning cluster, because the system has 120 molecules. For $\lambda = 5$ and $\lambda = 7$, a persistent percolation network does not form. The maximum cluster size can contain fewer than half of all the molecules for some time during the simulation, while spanning clusters do form at other times. This is similar to the picture presented by Vishnyakov and Neimark²¹ of transient bridges forming between large clusters. Our simulations show that such behavior is encountered near the percolation threshold. For $\lambda \geq 9$, a spanning cluster is present all the time. In this case, a connected water network permeates through the Nafion membrane at all times. Such a network is needed for effective proton conduction during fuel cell operation.

It is tempting to interpret the present results in terms of a phase transition model that postulates a transition, from water sorbed in the polymer matrix at low hydration levels to a phase-separated system consisting of a large water cluster and the polymer, as an energy barrier is surmounted. Oleinikova et al.⁵⁵ have pointed out that the relationship between the percolation threshold and the occurrence of any phase transition is poorly understood. Gebel⁵⁶ has argued, on the basis of continuous evolution of small-angle X-ray and neutron scattering spectra with increasing hydration level, that the percolation of the aggregates of ionic groups and water molecules is not due to a first-order transition. Our simulation also shows, as discussed previously,²⁶ that the separation into hydrophilic and hydrophobic regions is evident at all λ values and is not brought about by changes in hydration level.

A caveat about the present work and similar MD simulation studies is that the relaxation time of the polymer is likely to be longer than the 2 ns time scale of the present simulation as indicated by Cui et al.²⁹ Brunello et al.⁵⁷ have stated that one must bear in mind this limitation of insufficient sampling of polymer chain conformations in simulations that run for only a few tens of nanoseconds due to limited computational resources. We must keep in mind that the proton dynamics and polymer dynamics occur on completely different scales. In future, we plan to systematically study the correlation of the chain end-to-end vector in simulations that run for 100 ns and to coarse-

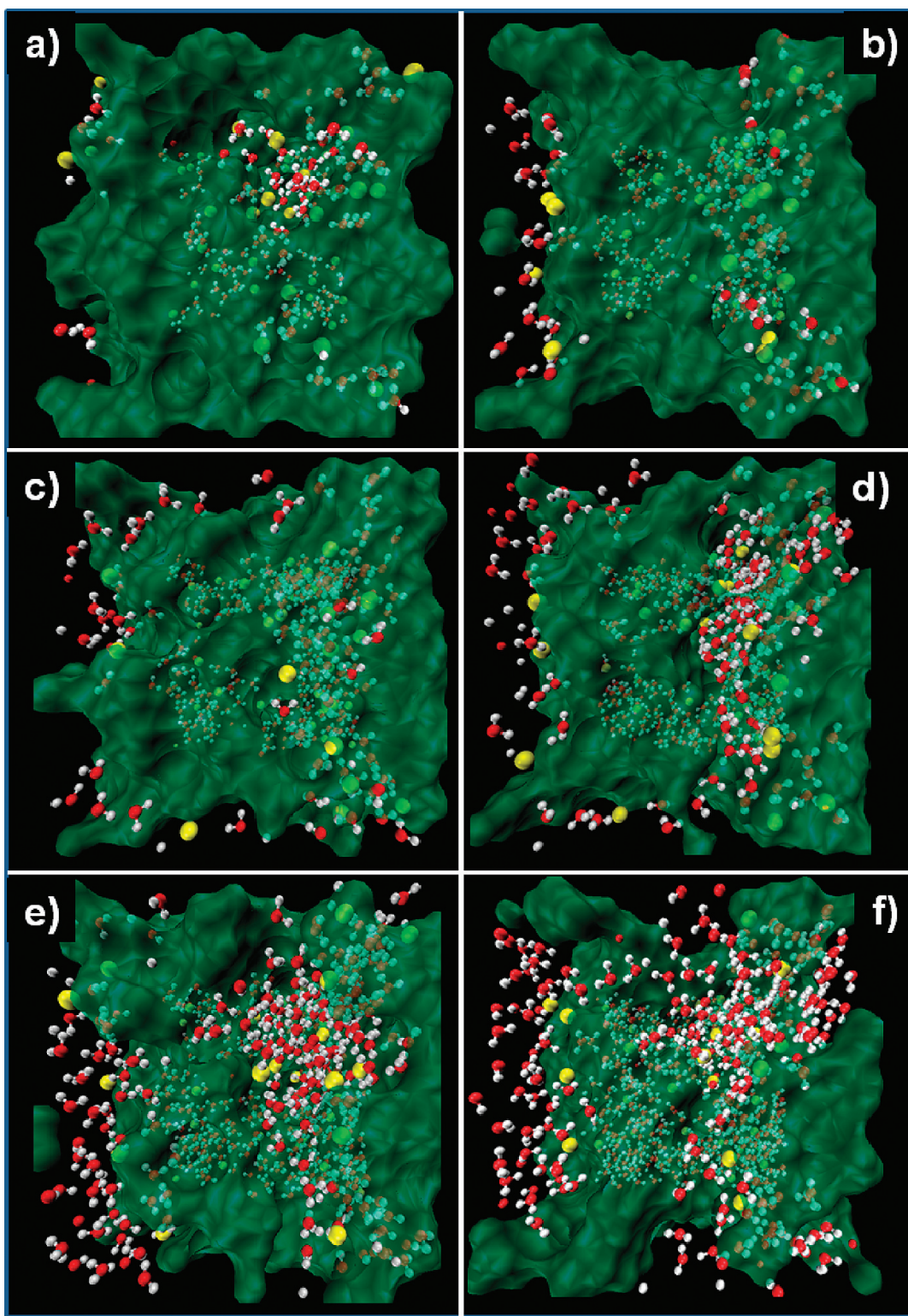


Figure 7. Perspective projection of H_2O molecules and H_3O^+ ions in Nafion for hydration level of (a) 3, (b) 5, (c) 7, (d) 9, (e) 11, and (f) 13.5. SO_3^- is shown as a large (yellow) bead. The backbone and pendant are shown as a transparent surface.

grain the force field to specifically study polymer conformations. Nonetheless, the present results establish a mathematical basis for the changes in electrical conductivity of Nafion membrane with increasing hydration level.⁸

In an effort to relate proton transport that underlies conductivity to the evolution of the water network in Nafion, we have used QHOP-MD and computed the dynamical properties of protons and time correlation functions. Consider a population operator, $h_i(t)$, where i refers to any proton acceptor site (all

water molecules are proton acceptors). A population operator $h_i(t)$ can be defined as follows:

$$h_i(t) = 1 \text{ if the proton resides on acceptor site } i \text{ at time } t; \\ h_i(t) = 0 \text{ otherwise.}$$

We define a correlation function $C(t)$, such that $C(t) = \langle h_i(0)|h_i(t)\rangle$, where $\langle \rangle$ denotes a statistical average over all i sites and over all configurations separated by time t . Figure 11a–c represents the time correlation function $[C(t)]$ corresponding to the decay of the proton population operator, which also

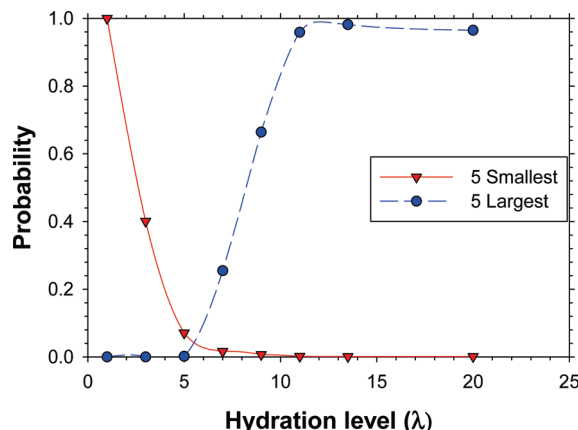


Figure 8. Probability of finding a H_2O molecule or H_3O^+ ion in the five smallest clusters (triangles) and five largest clusters (circles) in the system.

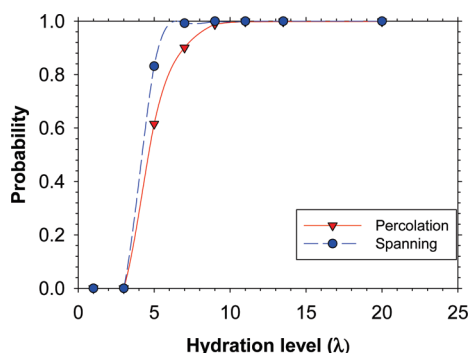


Figure 9. Probability of percolation (diamonds) and a spanning cluster (triangles) in Nafion as a function of hydration level.

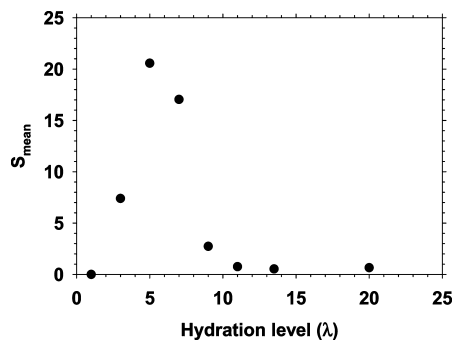


Figure 10. Mean cluster size (excluding the largest cluster) in Nafion as a function of hydration level.

represents the lifetime of a proton on any given site. A comparison of the decay of proton lifetimes in Figure 11a–c shows that the decay is faster at higher hydration ($\lambda = 15$) as compared to that at lower hydration ($\lambda = 5$) at 300 and 350 K. For a given temperature, the decay times show that the proton hops faster with increasing hydration. Further, at each level of membrane hydration, the decay of the proton is faster at 350 K than at 300 K. These results indicate that the structural diffusion of protons increases with hydration and temperature.

We quantified this result by computing the mean residence time (MRT) of the proton from the time correlation function $C(t)$. The MRT is obtained by representing the time correlation function $C(t)$ as a single-exponential function $\exp(-t/t_{\text{MR}})$, where t_{MR} represents the MRT of the proton on a water molecule. The natural logarithm of $C(t)$ for various levels of membrane hydration and temperature is displayed in Figure 11d–f. The slope of a linear fit to this logarithmic function gives the MRT.

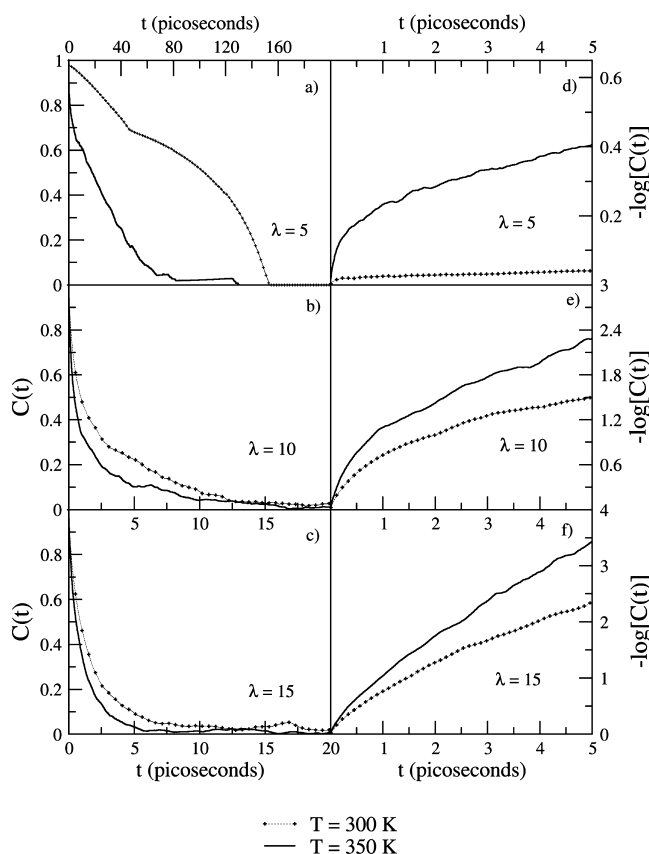


Figure 11. Correlation function [$C(t)$], and logarithm of correlation function [$-\log(C(t))$] for the residence time of a hopping proton at (a,d) $\lambda = 5$, (b,e) $\lambda = 10$, and (c,f) $\lambda = 15$.

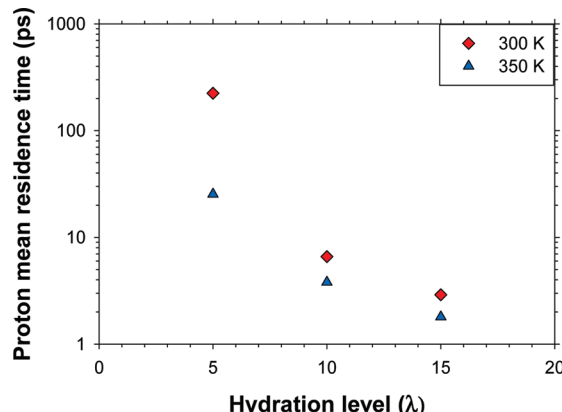


Figure 12. Proton mean residence time on a H_2O molecule in Nafion as a function of hydration level at temperatures 300 and 350 K.

of the proton. It should be noted that $\log(C(t))$ is nonlinear for short time scales (below 2 ps). This may be due to the fluctuations arising from the inherent definition of the population operator $h_i(t)$. Hence, the linear fit was extracted over the time period beyond the initial 2 ps.

Figure 12 shows the calculated MRTs of proton at 300 K (diamonds) and 350 K (triangles). The MRT decreases by 2 orders of magnitude when λ is increased from 5 to 10 at 300 K. The corresponding decrease at 350 K is by an order of magnitude. The value of MRT at 300 K for $\lambda = 5$ is very high. The $C(t)$ in Figure 11a does not decay to zero in the time of the simulation and statistical convergence of this quantity is poor for $t > 40$ ps at 300 K as compared to that at 350 K. This is because the proton remains attached to an acceptor water molecule for a very long time at 300 K, which was not the case

at 350 K. A similar observation was also reported by Petersen et al.¹⁹ who suggested the “caging effect” of classical hydroniums at lower hydration level as a possible explanation. This caging effect can be visualized in Figure 2. The decrease in proton MRT with increasing hydration is due to the formation of a three-dimensional percolating water network along which proton transport can occur. Recently, tightly connected water wires have been shown to facilitate proton transport towards the entrances of proton pumping proteins.¹

The rate constants (k) for proton hop between H_2O molecules were determined from the MRT of the proton according to the relationship $k = 1/\tau$. The computed rate constants at 300 K are 0.004, 0.152, and 0.345 ps^{-1} for $\lambda = 5, 10$, and 15, respectively. The corresponding rate constants at 350 K are 0.039, 0.263, and 0.556 ps^{-1} , respectively. The experimental NMR rate constant⁵⁸ for proton transfer in bulk water at 300 K is 0.63 ps^{-1} . Since the rate constants are inversely related to MRTs, the rate constants increase with increasing hydration and temperature. For illustration purposes, apparent activation energies were computed using the Arrhenius equation, $k = \exp(-E_A/RT)$, where E_A corresponds to the activation energy of the process of proton transfer from a H_3O^+ ion to a H_2O molecule. The activation energy computed for proton transfer at $\lambda = 5$ is ~ 9.5 kcal/mol. This high value of E_A is due to the small rate constant at 300 K, but may also be subject to limited sampling. However, the activation energies computed at $\lambda = 10$ and $\lambda = 15$ are 2.3 and 2.0 kcal/mol respectively, and hence only show an energy difference of ~ 0.3 kcal/mol. These values are in good agreement with the activation energy for proton transfer in bulk water estimated to be 2–3 kcal/mol.¹⁰ Since we have computed rate constants only for two temperatures, the calculated activation energies provide only a rough estimate. Nevertheless, they provide us a good benchmark for a more rigorous and detailed study on the kinetics of proton transport. Better sampling is required to compute accurate activation energies at low hydration and temperature.

We have also examined the mean square displacement (MSD) and diffusion coefficients of the proton at $\lambda = 15$. The MSD of the proton could not be fitted to a straight line at $\lambda = 5$ and 10, indicating that our simulations were not sufficiently long to observe steady-state diffusion at low hydration levels given the long proton residence times. Therefore, diffusion coefficients could not be reliably estimated at low hydration levels when the level of solvation around a proton is small. A previous study by Jang and Goddard⁴⁰ that used a similar approach to Q-HOP MD had also reported proton diffusion in Nafion only for $\lambda = 15$. Their value is about $0.7 \times 10^{-5} \text{ cm}^2/\text{s}$. We estimated the diffusion coefficient of the proton for $\lambda = 15$ to be $1.1 \times 10^{-5} \text{ cm}^2/\text{s}$ at both 300 and 350 K. The qualitative features of MSD at 300 and 350 K were found to be similar, which suggests that proton transfer and transport mechanisms remained unchanged within this temperature range. Our estimate is in general agreement with the simulations of Jang and Goddard⁴⁰ and the experimental conductivity measurements of Zawodinski et al.⁸ that yielded a proton diffusion coefficient of $\sim 1.3 \times 10^{-5} \text{ cm}^2/\text{s}$. For comparison, the diffusion coefficient of an excess proton in bulk water calculated by Q-HOP MD is $9.3 \times 10^{-5} \text{ cm}^2/\text{s}$ and the experimental value is also $9.3 \times 10^{-5} \text{ cm}^2/\text{s}$.³⁵

By performing a detailed percolation analysis of Nafion for a large number of λ values and relating the changes in water network to proton transport, the present study has provided quantitative information about the evolution of water clusters in Nafion membrane with increasing hydration level. These results shed light on experimental observations that indicate

abrupt changes in the dielectric constant,⁴⁶ conductivity,⁸ and water uptake⁵⁹ of Nafion around $\lambda = 6$. Lu et al.⁴⁶ performed dielectric relaxation spectroscopy of Nafion 117 and interpreted their results in terms of loosely bound water for $\lambda = 9$. They proposed that water molecules may reside in the hydrophilic paths connecting the hydrated ionic clusters. The present simulations reveal such a picture at high hydration levels and point to the important role of the SO_3^- group in facilitating the connection between water clusters. At the same time, our results show that near the percolation threshold the water in Nafion segregates into bound water clusters that are transiently connected by free and loosely bound water molecules. Our previous work²⁶ has quantified the relative proportions of bound, loosely bound, and free water molecules and showed that the fraction of free water increases with increasing λ .

Laporta et al.⁴ examined the structure of water in Nafion membranes using Fourier transform infrared spectroscopy (FT-IR). They suggested that the first H_2O molecules ($\lambda \leq 2$) dissociate the SO_3^- groups forming H_3O^+ ions, the next H_2O molecules solvate these ions forming water clusters of five or six molecules, and that higher hydration levels lead to the growth and aggregation of clusters and the formation of a continuous water phase. The percolation threshold calculated in the current simulation ($\lambda = 5$ to 6) agrees excellently with the value estimated from the experiments of Laporta et al.⁴ Our previous results²⁶ have showed that the average distance from a S atom within which another S atom can be found increases from 5.3 to 6.5 Å, the average number of H_3O^+ ions within the first hydration shell of the SO_3^- group decreases from about 2.5 to about 1.1, and the average H_2O molecule moves out of the first hydration shell of the SO_3^- group as λ increases from 1 to 7. When viewed in light of the above results, the present percolation and proton-hopping analysis sheds light on the dynamical processes underlying the formation of the water network in the complex chemical environment of a fuel cell membrane. This study has presented a rigorous protocol for comparing water uptake and conductivity of different membranes, and to make predictions about proposed membranes.

IV. Conclusions

We have used percolation analysis following classical molecular dynamics simulations to examine water clustering, connectivity of clusters, and persistence of spanning clusters as a function of hydration level in Nafion membrane. We have also used quantum hopping (Q-HOP) molecular dynamics method to compute the mean residence times (MRTs), rate constants, and activation energies for proton transfer. At low hydration levels ($\lambda \leq 5$), clusters of water molecules and hydronium ions are isolated from each other and proton residence time on a water molecule is about 220 ps at 300 K. The average number of clusters decreases from more than 25 for $\lambda = 3$ to fewer than 4 for $\lambda = 7$. Multiple SO_3^- groups confine the H_3O^+ ion. Vehicular proton transport is hindered by steric hindrance and long-range structural transport is not possible due to the lack of connectivity of H_2O molecules.

Water network percolation occurs between $\lambda = 5$ and $\lambda = 6$ in agreement with estimates based on infrared spectroscopy experiments. This threshold was determined on the basis of multiple criteria. In fact, we have proposed a new criterion for detecting percolation based on the relative probabilities of finding water molecules in the smallest and largest clusters. Near the percolation threshold, clusters are linked from time to time by mobile H_2O molecules, so that transient spanning clusters form and disappear. At high hydration levels ($\lambda \geq 9$), a persistent

spanning cluster permeates the membrane and creates water channels along which the proton can hop. At high λ , the proton residence time on a H₂O molecule drops by 2 orders of magnitude from the value at low λ to a few picoseconds. Our Q-HOP simulations show faster proton transfer with increasing hydration and temperature. At higher hydration, the faster proton transfer is due to ease of solvation of the proton, whereas at higher temperatures, protons are more mobile because thermal effects generate a larger number of favorable proton transfer geometries. At high λ , the rate constants approach that of proton transfer in bulk water. The proton diffusion coefficient for $\lambda = 15$ at 300 K is about 1.1×10^{-5} cm²/s in good agreement with experiment. The understanding of water percolation and dynamics of proton transfer generated by this work could help in the design of future polymer membrane materials that have lower uptake of water and yet offer faster proton transfer and transport.

Acknowledgment. This work was supported by the U.S. Department of Energy's (DOE) Office of Basic Energy Sciences, Chemical Sciences, Geosciences and Biosciences Division, under Contract DE-AC05-76RL01830. It was performed in part using the Molecular Science Computing Facility (MSCF) in the EMSL, a national scientific user facility sponsored by DOE's Office of Biological and Environmental Research located at Pacific Northwest National Laboratory (PNNL). PNNL is operated by Battelle for DOE. This work benefited from resources of the National Energy Research Scientific Computing Center, which is supported by the Office of Science of DOE under Contract No. DE-AC02-05CH1123. This work also used computing resources provided by the Chemical & Materials Sciences Division at PNNL. VH and WG thank DFG for funding the development of the Q-HOP method.

References and Notes

- (1) Gu, W.; Helms, V. *J. Am. Chem. Soc.* **2009**, *131*, 2080–2081.
- (2) Devanathan, R. *Energy Environ. Sci.* **2008**, *1*, 101–119.
- (3) Mauritz, K. A.; Moore, R. B. *Chem. Rev.* **2004**, *104*, 4535–4585.
- (4) Laporta, M.; Pegoraro, M.; Zanderighi, L. *Phys. Chem. Chem. Phys.* **1999**, *1*, 4619–4628.
- (5) Gruger, A.; Regis, A.; Schmatko, T.; Colomban, P. *Vibr. Spectros.* **2001**, *26*, 215–225.
- (6) Paddison, S. J. *J. New Mater. Electrochem. Syst.* **2001**, *4*, 197–207.
- (7) Schmidt-Rohr, K.; Chen, Q. *Nat. Mater.* **2008**, *7*, 75–83.
- (8) Zawodzinski, T. A.; Davey, J.; Valerio, J.; Gottesfeld, S. *Electrochim. Acta* **1995**, *40*, 297–302.
- (9) Kreuer, K.-D.; Paddison, S. J.; Spohr, E.; Schuster, M. *Chem. Rev.* **2004**, *104*, 4637–4678.
- (10) Agmon, N. *Chem. Phys. Lett.* **1995**, *244*, 456–462.
- (11) Marx, D. *ChemPhysChem* **2006**, *7*, 1848–1870.
- (12) Elliott, J. A.; Paddison, S. J. *Phys. Chem. Chem. Phys.* **2007**, *9*, 2602–2618.
- (13) Paddison, S. J.; Elliott, J. A. *J. Phys. Chem. A* **2005**, *109*, 7583–7593.
- (14) Glezakou, V.-A.; Dupuis, M.; Mundy, C. *J. Phys. Chem. Chem. Phys.* **2007**, *9*, 5752–5760.
- (15) Roudgar, A.; Narasimhachary, S. P.; Eikerling, M. *Chem. Phys. Lett.* **2008**, *457*, 337–341.
- (16) Choe, Y.-K.; Tsushima, E.; Ikeshoji, T.; Yamakawa, S.; Hyodo, S. *Phys. Chem. Chem. Phys.* **2009**, *11*, 3892–3899.
- (17) Spohr, E.; Commer, P.; Kornyshev, A. A. *J. Phys. Chem. B* **2002**, *106*, 10560–10569.
- (18) Kornyshev, A. A.; Kuznetsov, A. M.; Spohr, E.; Ulstrup, J. *J. Phys. Chem. B* **2003**, *107*, 3351–3366.
- (19) Petersen, M. K.; Wang, F.; Blake, N. P.; Metiu, H.; Voth, G. A. *J. Phys. Chem. B* **2005**, *109*, 3727–3730.
- (20) Paul, R.; Paddison, S. J. *J. Chem. Phys.* **2005**, *123*, 224704.
- (21) Vishnyakov, A.; Neimark, A. V. *J. Phys. Chem. B* **2001**, *105*, 9586–9594.
- (22) Urata, S.; Irisawa, J.; Takada, A.; Shinoda, W.; Suzuki, S.; Mikami, M. *J. Phys. Chem. B* **2005**, *109*, 4269–4278.
- (23) Jang, S. S.; Molinero, V.; Cağın, T.; Goddard, W. A. *J. Phys. Chem. B* **2004**, *108*, 3149–3157.
- (24) Blake, N. P.; Mills, G.; Metiu, H. *J. Phys. Chem. B* **2007**, *111*, 2490–2494.
- (25) Venkatnathan, A.; Devanathan, R.; Dupuis, M. *J. Phys. Chem. B* **2007**, *111*, 7234–7244.
- (26) Devanathan, R.; Venkatnathan, A.; Dupuis, M. *J. Phys. Chem. B* **2007**, *111*, 8069–8079.
- (27) Devanathan, R.; Venkatnathan, A.; Dupuis, M. *J. Phys. Chem. B* **2007**, *111*, 13006–13113.
- (28) Knox, C. K.; Voth, G. A. *J. Phys. Chem. B* **2010**, *114*, 3205–3218.
- (29) Cui, S.; Liu, J.; Selvan, M. E.; Keffer, D. J.; Edwards, B. J.; Steele, W. V. *J. Phys. Chem. B* **2007**, *111*, 2208–2218.
- (30) Cui, S.; Liu, J.; Selvan, M. E.; Paddison, S. J.; Keffer, D. J.; Edwards, B. J. *J. Phys. Chem. B* **2008**, *112*, 13273–13284.
- (31) Wescott, J. T.; Qi, Y.; Subramanian, L.; Capehart, T. W. *J. Chem. Phys.* **2006**, *124*, 134702.
- (32) Malek, K.; Eikerling, M.; Wang, Q.; Liu, Z.; Otsuka, S.; Akizuki, K.; Abe, M. *J. Chem. Phys.* **2008**, *129*, 204702.
- (33) Morris, D. R.; Sun, X. *J. Appl. Polym. Sci.* **1993**, *50*, 1445–1452.
- (34) Brovchenko, I.; Krukauf, A.; Oleinikova, A.; Mazur, A. K. *J. Am. Chem. Soc.* **2008**, *130*, 121–131.
- (35) Lill, M. A.; Helms, V. *J. Chem. Phys.* **2001**, *115*, 7993–8005.
- (36) Gu, W.; Frigato, T.; Straatsma, T. P.; Helms, V. *Angew. Chem. Int. Ed.* **2007**, *46*, 2939–2943.
- (37) Gu, W.; Helms, V. *ChemPhysChem* **2007**, *8*, 2445–2451.
- (38) De Groot, B. L.; Frigato, T.; Helms, V.; Grubmüller, H. *J. Mol. Biol.* **2003**, *333*, 279–293.
- (39) Lill, M. A.; Helms, V. *Proc. Natl. Acad. Sci.* **2002**, *99*, 2778–2781.
- (40) Jang, S. S.; Goddard III, W. A. *J. Phys. Chem. C* **2007**, *111*, 2759–2769.
- (41) Lill, M. A.; Helms, V. *J. Chem. Phys.* **2001**, *114*, 1125–1132.
- (42) Lill, M. A.; Helms, V. *J. Chem. Phys.* **2001**, *115*, 7985–7992.
- (43) Todorov, I. T.; Smith, W.; Trachenko, K.; Dove, M. T. *J. Mater. Chem.* **2006**, *16*, 1911–1918.
- (44) Mayo, S. L.; Olafson, B. D.; Goddard, W. A. *J. Phys. Chem.* **1990**, *94*, 8897–8909.
- (45) Levitt, M.; Hirshberg, M.; Sharon, R.; Laidig, K. E.; Daggett, V. *J. Phys. Chem. B* **1997**, *25*, 5051–5061.
- (46) Lu, Z.; Polizos, G.; Macdonald, D. D.; Manias, E. *J. Electrochem. Soc.* **2008**, *155*, B163–B171.
- (47) Pártay, L. B.; Jedlovzky, P.; Brovchenko, I.; Oleinikova, A. *Phys. Chem. Chem. Phys.* **2007**, *9*, 1341–1346.
- (48) Rintoul, M. D.; Torquato, S. *J. Phys. A: Math. Gen.* **1997**, *30*, L585–L592.
- (49) Bylaska, E. J.; de Jong, W. A.; Kowalski, K.; Straatsma, T. P.; Valiev, M.; Wang, D.; Aprà, E.; Windus, T. L.; Hirata, S.; Hackler, M. T.; Zhao, Y.; Fan, P.-D.; Harrison, R. J.; Dupuis, M.; Smith, D. M. A.; Nieplocha, J.; Tipparaju, V.; Krishnan, M.; Auer, A. A.; Nooijen, M.; Brown, E.; Cisneros, E.; Fann, G. I.; Frücht, H.; Garza, J.; Hirao, K.; Kendall, R.; Nichols, J. A.; Tseneckman, K.; Wolinski, K.; Anchell, J.; Bernholdt, D.; Borowski, P.; Clark, T.; Clerc, D.; Dachsel, H.; Deegan, M.; Dyall, K.; Elwood, D.; Glendening, E.; Gutowski, M.; Hess, A.; Jaffe, J.; Johnson, B.; Ju, J.; Kobayashi, R.; Kutteh, R.; Lin, Z.; Littlefield, R.; Long, X.; Meng, B.; Nakajima, R.; Niu, S.; Pollack, L.; Rosing, M.; Sandrone, G.; Stave, M.; Taylor, H.; Thomas, G.; van Lenthe, J.; Wong, A.; Zhang, Z. *NWChem, A Computational Chemistry Package for Parallel Computers, Version 4.7*; Pacific Northwest National Laboratory: Richland, WA, 2006.
- (50) Kendall, R. A.; Apra, E.; Bernholdt, D. E.; Bylaska, E. J.; Dupuis, M.; Fann, G. I.; Harrison, R. J.; Ju, J.; Nichols, J. A.; Nieplocha, J.; Straatsma, T. P.; Windus, T. L.; Wong, A. T. *Comput. Phys. Commun.* **2000**, *128*, 260–283.
- (51) Berendsen, H. J. C.; Grigera, J. R.; Straatsma, T. P. *J. Phys. Chem.* **1987**, *91*, 6269–6271.
- (52) Wang, J.; Cieplak, P.; Kollman, P. A. *J. Comput. Chem.* **2000**, *21*, 1049–1074.
- (53) Wang, J.; Wolf, R. M.; Caldwell, J. W.; Kollman, P. A.; Case, D. A. *J. Comput. Chem.* **2004**, *25*, 1157–1174.
- (54) Allen, M. P.; Tildesley, D. J. *Computer Simulation of Liquids*; Oxford University Press: New York, 1987; Chapter 2.
- (55) Oleinikova, A.; Brovchenko, I.; Geiger, A.; Guillot, B. *J. Chem. Phys.* **2002**, *117*, 3296–3304.
- (56) Gebel, G. *Polymer* **2000**, *41*, 5829–5838.
- (57) Brunello, G.; Lee, S. G.; Jang, S. S.; Qi, Y. *J. Renewable Sustainable Energy* **2009**, *1*, 033101.
- (58) Meiboom, S. *J. Chem. Phys.* **1961**, *34*, 375–388.
- (59) Zawodzinski, T. A.; Derouin, C.; Radzinski, S.; Sherman, R. J.; Smith, V. T.; Springer, T. E.; Gottesfeld, S. *J. Electrochem. Soc.* **1993**, *140*, 1041–1047.